AEM
Journals.ASM.org

The Antimicrobial Mechanism of Action of Epsilon-Poly-L-Lysine

Morten Hyldgaard,[a,b] Tina Mygind,[b] Brian S. Vad,[a,c] Marcel Stenvang,[a,c] Daniel E. Otzen,[a,c] Rikke L. Meyer[a,d]

Interdisciplinary Nanoscience Center, Aarhus University, Aarhus, Denmark[a]; DuPont, Brabrand, Denmark[b]; Department of Molecular Biology and Genetics, Aarhus University, Aarhus, Denmark[c]; Department of Bioscience, Aarhus University, Aarhus, Denmark[d]

Epsilon-poly-L-lysine (ε-PL) is a natural antimicrobial cationic peptide which is generally regarded as safe (GRAS) as a food preservative. Although its antimicrobial activity is well documented, its mechanism of action is only vaguely described. The aim of this study was to clarify ε-PL's mechanism of action using *Escherichia coli* and *Listeria innocua* as model organisms. We examined ε-PL's effect on cell morphology and membrane integrity and used an array of *E. coli* deletion mutants to study how specific outer membrane components affected the action of ε-PL. We furthermore studied its interaction with lipid bilayers using membrane models. *In vitro* cell studies indicated that divalent cations and the heptose I and II phosphate groups in the lipopolysaccharide layer of *E. coli* are critical for ε-PL's binding efficiency. ε-PL removed the lipopolysaccharide layer and affected cell morphology of *E. coli*, while *L. innocua* underwent minor morphological changes. Propidium iodide staining showed that ε-PL permeabilized the cytoplasmic membrane in both species, indicating the membrane as the site of attack. We compared the interaction with neutral or negatively charged membrane systems and showed that the interaction with ε-PL relied on negative charges on the membrane. Suspended membrane vesicles were disrupted by ε-PL, and a detergent-like disruption of *E. coli* membrane was confirmed by atomic force microscopy imaging of supported lipid bilayers. We hypothesize that ε-PL destabilizes membranes in a carpet-like mechanism by interacting with negatively charged phospholipid head groups, which displace divalent cations and enforce a negative curvature folding on membranes that leads to formation of vesicles/micelles.

Food poisoning microorganisms cause annually more than one billion gastrointestinal tract inflammations and an estimated 5 to 13 million deaths (1, 2). The safety of traditional preservatives has been questioned in the last few years, so to meet the consumers demand and at the same time ensure food safety, the food industry is turning to natural antimicrobials as preservatives. ε-Poly-L-lysine (ε-PL) is a promising natural antimicrobial that has a broad spectrum of activity against food spoilage and food-poisoning bacteria *in vitro* (3–5) and in complex food matrices (6, 7).

Biosynthesized ε-PL is a hydrophilic cationic linear homo-poly-amino acid typically composed of 25 to 35 identical L-lysine residues with an isoelectric point around 9.0 and is described as having a peptide bond between carboxyl groups and ε-amino groups of L-lysine residues rather than the conventional peptide bonds linking α-poly-L-lysine (α-PL) (8). ε-PL is produced by a membrane-bound ε-PL synthetase that has the characteristics of nonribosomal peptide synthetases, which does not bind the elongating ε-PL chain covalently during polymerization (9). The variable chain lengths of ε-PL is thus stemming from the continues polymerization of ε-PL, which at any time point can diffuse into solution having a random number of residues (9).

It is recognized that ε-PL's antimicrobial activity is closely related to the number of repetitive L-lysine residues, and it has been shown that >10 residues are required for ε-PL to exert proper antibacterial activity (3, 10). Interestingly, the ε-PL is a more potent antimicrobial compound than α-PL (3), but the reason for this difference is unknown.

The antimicrobial activity of ε-PL was recognized more than 30 years ago, and in Japan it has been approved as a food preservative since the late 1980s (11, 12). Since ε-PL's discovery in the 1970s, it has been approved by the U.S. Food and Drug Administration in 2004 for use in boiled rice in the United States and, as described in the generally regarded as safe (GRAS) notifications 135 and 336, ε-PL can currently be applied to an assortment of food products such as soft drinks, cheese, egg-based dishes, salad dressings, fish, sauces, potato-based foods, etc. ε-PL was first biosynthesized and isolated from culture filtrates of *Streptomyces albulus* (12) and is now industrially produced by aerobic fermentation using a *S*-(2-aminoethyl)-L-cysteine mutant derived from *S. albulus* 11011A (8). The addition of large amounts of ε-PL to food products results in a bitter taste but remains safe for humans to consume since ε-PL is biodegradable without any cytotoxicity (8, 13). Furthermore, ε-PL has been suggested to have an anti-obesity action because it can suppress dietary fat absorption from the small intestine by inhibiting pancreatic lipase activity even after incubation with digestive enzymes such as trypsin, α-chymotrypsin, and pepsin (14).

More detailed knowledge about the mode of antimicrobial action can be used to increase the efficacy of an antimicrobial and help prevent the development of bacterial resistance (15). The mechanism of action of ε-PL has not been fully investigated, but it has been proposed that adsorption of ε-PL to the cell surface plays an important role (3). It has been suggested that the cationic polypeptide interacts with the negatively charged cell surface by ionic adsorption and that ε-PL subsequently interferes with cell membranes in a reaction that has been proposed to include stripping of the lipopolysaccharide (LPS) layer that leads to a permeabilization

Received 9 July 2014 **Accepted** 30 September 2014
Published ahead of print 10 October 2014
Editor: J. Björkroth
Address correspondence to Rikke L. Meyer, rikke.meyer@inano.au.dk.
Supplemental material for this article may be found at http://dx.doi.org/10.1128/AEM.02204-14.

doi:10.1128/AEM.02204-14

of the outer membrane (3, 16). This could be the case as the cationic ε-PL probably would interact with the outer membrane of Gram-negative bacteria which contains hydrophobic and negatively charged LPS that create an effective barrier toward macromolecules and lipophilic compounds (17, 18). However, conclusive evidence for the proposed hypotheses together with the molecular mechanism of action of ε-PL on the cytoplasmic membrane is still lacking.

The antimicrobial mechanism of action for cationic peptides has generally been described by three models known as barrel-stave, toroidal, and carpet mechanism. The barrel-stave mechanism requires direct contact with the hydrophobic core of bilayers, whereas the other two mechanisms only involve interaction with the membrane surface or headgroup region (19, 20). In the toroidal pore mechanism, the hydrophobic residues displace phospholipid headgroups and enforce positive membrane curvature where the pore lumen is formed by both peptide and phospholipid head groups (19, 20). In the carpet mechanism, membranes are permeabilized in a nonspecific detergent-like manner; this only requires interaction of the peptides with the headgroup region of phospholipids where they interact with negatively charged lipids (19, 21). Although these three mechanisms are generally accepted, they are too rigid to explain all interactions taking place in a complex membrane, and therefore other models need to be considered (20). Some of these models are the disordered toroidal pore model (22), the electroporation model, the sinking raft model (23), and the grip-and-dip model (24). It should also be noted that the mechanism by which peptides interact with membranes is not only determined by the peptide or membrane composition of headgroups but also the type of acyl-chains present in the membrane (25).

In the present study, we aimed to increase our understanding of ε-PL's mechanism of action at the molecular level using *Escherichia coli* and *Listeria innocua* as model organisms, and different lipid extract compositions to mimic ε-PL's interaction with the cytoplasmic cell membrane. We used the nonpathogenic Gram-negative *E. coli* K-12 as a model organism for pathogenic *E. coli* strains, which are a common problem in the food industry and causes many hospitalizations of consumers each year (26). The Gram-positive *L. innocua* is food-associated and closely related to the pathogenic *Listeria monocytogenes* (27).

MATERIALS AND METHODS

Chemicals. Standard chemicals were purchased from Sigma-Aldrich. ε-PL powder consisted of 50% ε-PL and 50% dextrin (Chisso Corp., Chiyoda-ku, Tokyo, Japan), and all concentrations are reported at the actual ε-PL content. Fluorescent stains—propidium iodide (PI; L7012 and L13152), Alexa Fluor 633 hydrazide (A30634), DiO (D275), and dextran labeled with Alexa Fluor 488 (D22910)—were acquired from Molecular Probes (Eugene, OR). Fluorescein (FITC)-labeled ε-PL was acquired from Guilin Peptide Technology, Ltd. (Guilin, China), and labeled with 0.005 mol of 5-FITC per mol of lysine monomer. 1,2-Dioleoyl-*sn*-glycero-3-phospho-(1′-*rac*-glycerol) (DOPG; 840475P), 1,2-dioleoyl-*sn*-glycero-3-phosphocholine (DOPC; 850375P), and *E. coli* polar lipid extract (100600C) were acquired from Avanti Polar Lipids, Inc. (Alabaster, AL).

Preparation of cultures. *E. coli* K-12 (LZB035; Blades Biological, Ltd., Cowden, Edenbridge, Kent, United Kingdom) and *L. innocua* (DSM 20649) were grown in either tryptic soy broth (TSB; pH 6.0) or TSB plus 1.5% tryptic soy agar (TSA). The parental strain, *E. coli* BW25113, and all isogenic deletion mutants were obtained from the Keio collection (28) of The Coli Genetic Stock Centre (Yale University), while *E. coli* JM109 was acquired from DSMZ (DSM 3423) (Table 1). Cells were cultured overnight at 25°C in TSB until exponential growth phase, which were assessed by having an optical density at 620 nm (OD_{620}) between 0.05 and 0.25. Cells were harvested by centrifugation (5,000 × *g*, 10 min), and pellets were resuspended to cell densities of 10^7 or 10^6 CFU/ml in sterile 2-(*N*-morpholino)ethanesulfonic acid (MES) buffer (pH 6), TSB, or Ringer's solution (Merck, Darmstadt, Germany). The bacterial culture density and resuspension liquid is defined for each experiment.

Measurement of cell surface charge. The cell surface charge of the wild-type and mutant strains was determined because variations between strains could affect their ability to interact with ε-PL. Triplicate bacterial cultures (10^7 CFU/ml) were prepared in sterile filtered (0.2-μm pore size) MES buffer or TSB. ε-PL stocks, bacterial suspensions, and MES buffer or TSB were mixed to final concentrations of 0 or 37 mg/liter ε-PL and a cell density of 5×10^5 CFU/ml. Samples were incubated 4 h at 25°C, harvested by centrifugation (5,000 × *g*, 10 min), and washed three times before resuspension in the appropriate solution. The zeta potentials were measured in a folded capillary cell (DTS 1070; Malvern Instruments, Worchestershire, United Kingdom) at 25°C using a Zetasizer Nano ZS (Malvern Instruments) equipped with a 633 He-Ne laser and controlled using Zetasizer software (v7.02). Cells were allowed to equilibrate for 120 s at 25°C before the zeta potential was measure three times for each replicate sample. The Smoluchowski equation was used to calculate the zeta potential from nine electrophoretic mobility measurements.

Evaluation of antimicrobial activity. (i) Inhibition of growth. The MICs of ε-PL against *E. coli* K-12 and *L. innocua* were determined by monitoring cell growth in 96-well flat-bottom microtiter plates (catalog no. 260887; Nunc plates; Thermo Scientific). Three replicate cultures of 10^7 CFU/ml in MES buffer were prepared for inoculation of the microtiter plate. Wells were filled with 100 μl of TSB, and ε-PL (dissolved in TSB) was then added from stock solutions in a 1.5-serial dilution. Finally, TSB and bacterial culture were added in order to obtain a final cell concentration of 5×10^5 CFU/ml and an ε-PL concentration ranging from 0 to 500 mg/liter for *E. coli* K-12 or 0 to 750 mg/liter for *L. innocua*. For *E. coli* wild-type strains and isogenic mutants, the final ε-PL concentrations ranged from 0 to 250 mg/liter in 12.5-mg/liter steps. Cell-free or ε-PL-free controls were incubated with the same volumes of TSB. Plates were incubated at 25°C, and the OD_{620} was monitored every 20 min for 24 h using a plate reader (Sunrise; Tecan, Männedorf, Switzerland). Because ε-PL contributed to the optical density, the OD_{620} signal from cell-free controls containing equal amounts of ε-PL were used as a reference when measuring the OD_{620} to monitor bacterial growth. We defined the MIC as the smallest ε-PL concentration resulting in an average increase of OD_{620} corresponding to <20% of the increase observed in ε-PL-free "growth controls."

(ii) Influence of divalent cations on the antimicrobial activity. We tested the influence of divalent cations on the antimicrobial activity of ε-PL against *E. coli* K-12 and *L. innocua*. Cells incubated with ε-PL in TSB (at the MIC) and with the addition of 0, 2.5, 5, 10, and 20 mM Mg^{2+} or Ca^{2+} ions. The OD_{620} was determined every 20 min for 24 h at 25°C.

Bactericidal effect. Absorbance measurements only identify inhibition of cell growth and do not provide information on cell viability changes. ε-PL's effect on cell viability over time while suspended in TSB was determined using the method of Miles et al. (29) and CFU counts. Triplicate bacterial suspensions with 10^7 CFU/ml were prepared in Ringer's solution. Bacterial suspensions were mixed with ε-PL dissolved in TSB to a final cell density of 5×10^5 CFU/ml and a final ε-PL concentration of 0, 1/2× MIC, MIC, or 2× MIC. The CFU was determined after 0, 2, 4, 8, 12, 16, 20, and 24 h of incubation at 25°C: 100 μl cell the suspension was serial diluted to 10^{-6} in Ringer's solution, and 20 μl from each serial dilution step was transferred to two TSA plates, followed by incubation at 25°C for 24 h before the CFU were counted.

Evaluation of antimicrobial mechanism of action. (i) Effect on cell structure. AFM was used to evaluate the effect of ε-PL on cell morphology. Cells were immobilized to coverslips using Cell-TAK cell and tissue

TABLE 1 MICs of ε-PL against parent strains and mutants detected in the range 0 to 250 mg/liter, except for *L. innocua*, and detected by optical density measurements of growth at 620 nm[a]

Strain	Genotype	Phenotype	MIC (mg/liter)	Mean zeta potential (mV) ± SD				Reference(s)
				TSB	TSB + ε-PL	MES	MES + ε-PL	
L. innocua		Wild type	750	**−11.61** [β]± **1.38**	−9.38 ± 0.71	**−33.86** [β]± **1.18**	10.00 ± 8.95	
E. coli								
K-12 (LZB035)		Wild type	74	**−13.1** [β]± **0.72**	−12.54 ± 0.65	**−45.97** [β]± **2.79**	9.92 ± 3.16	
D21	F⁻ *proA23 lac-28 tsx-81 trp-30 his-51 rpsL173*(*strR*) *ampCp-1*	Parental wild-type that expresses core portion of LPS	87.5	**−13.31** [β]± **0.44**	−12.12 ± 1.37*	**−51.1** [β]± **1.13**	22.31 ± 2.31	50–52
JM109	F′ *traD36 proAB laqI*^{q}*ZΔ*M15) *recA1 endA1 gyrA96 thi hsdR17 supE44 relA1* λ⁻ Δ(*lac-proAB*)	Expresses full core portion of the LPS and has an extended O-antigen polysaccharide chain; O-rough:H48	87.5	−13.72 ± 0.5	**−14.61** ± **0.51**	**−51.6** [β]± **5.9**	20.56 ± 2.77	50, 53
D21f2	F⁻ *proA23 lac-28 tsx-81 trp-30 his-51 rpsL173*(*strR*) *rfa-31 rfa-1 ampCp-1*	Truncated LPS after the Kdo carboxyl group	112.5	**−15.66** [β]± **0.74***	−13.9 ± 1.05	**−41.4** [β]± **5.47***	10.33 ± 7.31*	51, 52
BW25113	F⁻ Δ(*araD-araB*)*567* Δ*lacZ4787* (::*rrnB-3*) λ⁻ *rph-1* Δ(*rhaD-rhaB*)*568 hsdR514*	Parent strain	87.5	−13 ± 0.75	−13.03 ± 1	**−51.3** [β]± **1.08**	26.97 ± 3.32	28, 36, 54
JW2039-1	F⁻ Δ(*araD-araB*)*567* Δ*lacZ4787* (::*rrnB-3*) λ⁻ Δ*wcaF752*::*kan rph-1* Δ(*rhaD-rhaB*)*568 hsdR514*	Knockout of capsular colanic acid biosynthesis acetyltransferase; less slime	87.5	−9.1 ± 0.6*	−9.73 ± 0.71*	**−52** [β]± **1.26**	25.26 ± 4.29	28, 41, 55
JW3595-2	F⁻ Δ(*araD-araB*)*567* Δ*lacZ4787* (::*rrnB-3*) λ⁻ Δ*rfaF732*::*kan rph-1* Δ(*rhaD-rhaB*)*568 hsdR514*	Inner core mutant with Kdo I and II and Hep I (Δ*waaF*)	162.5	−12.3 ± 0.86	−12.43 ± 0.63	**−53.3** [β]± **1.17***	24.6 ± 2.71	56, 57
JW3596-1	F⁻ Δ(*araD-araB*)*567* Δ*lacZ4787* (::*rrnB-3*) λ⁻ Δ*rfaC733*::*kan rph-1* Δ(*rhaD-rhaB*)*568 hsdR514*	Inner core mutant with Kdo I and II and no Hep I, II, or III (Δ*waaC*)	137.5	**−17.74** [β]± **0.96***	−15.04 ± 2.16*	**−48.49** [β]± **5.45**	10.63 ± 2.37*	36, 57
JW3597-1	F⁻ Δ(*araD-araB*)*567* Δ*lacZ4787* (::*rrnB-3*) λ⁻ Δ*rfaL734*::*kan rph-1* Δ(*rhaD-rhaB*)*568 hsdR514*	Lacks O-antigen and cannot ligate colanic acid to the LPS core (Δ*waaL*)	87.5	**−13.18** [β]± **0.9**	−11.77 ± 1.12*	**−49.16** [β]± **1.83***	23.09 ± 3.91*	58, 59
JW3600-1	F⁻ Δ(*araD-araB*)*567* Δ*lacZ4787* (::*rrnB-3*) λ⁻ Δ*rfaY736*::*kan rph-1* Δ(*rhaD-rhaB*)*568 hsdR514*	Dephosphorylated Hep II; has Kdo I and II and Hep I, II, and III (Δ*waaY*)	162.5	−14.16 ± 1.43	−13 ± 0.93	**−51.06** [β]± **1.16**	23.59 ± 2.98*	38
JW3605-1	F⁻ Δ(*araD-araB*)*567* Δ*lacZ4787* (::*rrnB-3*) λ⁻ Δ*rfaP741*::*kan rph-1* Δ(*rhaD-rhaB*)*568 hsdR514*	Has Kdo I and II and dephosphorylated Hep I and II (Δ*waaP*)	162.5	−11.96 ± 1.43	−13.13 ± 1.27	**−47.33** [β]± **1.25***	−2.81 ± 0.99*	36, 38
JW3606-1	F⁻ Δ(*araD-araB*)*567* Δ*lacZ4787* (::*rrnB-3*) λ⁻ Δ*rfaG742*::*kan rph-1* Δ(*rhaD-rhaB*)*568 hsdR514*	No outer core; has Kdo I and II and Hep I, II, and III; dephosphorylated Hep II and 40% of Hep I have phosphate substitution (Δ*waaG*)	150	**−19.53** [β]± **1.19***	−15.23 ± 0.9*	**−55.07** [β]± **1.93***	18.83 ± 3.10*	36, 39, 56
JW3607-2	F⁻ Δ(*araD-araB*)*567* Δ*lacZ4787* (::*rrnB-3*) λ⁻ Δ*rfaQ743*::*kan rph-1* Δ(*rhaD-rhaB*)*568 hsdR514*	Inner core mutant with Kdo I and II and Hep I and dephosphorylated Hep II (Δ*waaQ*)	175	−13.69 ± 1.17	−14.2 ± 0.54*	**−55.47** [β]± **1.54***	25.62 ± 2.81	38, 56
JW4277-1	F⁻ Δ(*araD-araB*)*567* Δ*lacZ4787* (::*rrnB-3*) λ⁻ *rph-1* Δ(*rhaD-rhaB*)*568* Δ*fimA782*::*kan hsdR514*	Lacks type I fimbriae	87.5	**−12.14** [β]± **0.65***	−11.38 ± 0.47*	**−48.68** [β]± **1.29***	21.61 ± 8.63*	55
JW5917-1	F⁻ Δ(*araD-araB*)*567* Δ*lacZ4787* (::*rrnB-3*) λ⁻ Δ*rcsC771*::*kan rph-1* Δ(*rhaD-rhaB*)*568 hsdR514*	Lacks negative regulatory gene of colanic acid synthesis; uncontrolled sliminess	175	−15.13 ± 0.79*	−14.76 ± 1.04*	**−51.36** [β]± **0.56**	22.41 ± 1.90*	55, 60

[a] Zeta potential measurements of bacteria suspended in TSB or MES buffer were determined at pH 6.0 treated with or without ε-PL (at ε-PL concentrations of 375 mg/liter against *L. innocua* and 37 mg/liter against *E. coli* strains and mutants for 4 h at 25°C, followed by washing steps. A Student *t* test was used to compare the zeta potential means of cells treated with or without ε-PL or to compare the means of mutants with their respective parent strain. Statistically significant differences ($P < 0.05$) between untreated and treated samples are indicated in boldface for the most negative value, while a zeta potential with a statistically significant difference from the parent strain is indicated by an asterisk. Boldfacing in the genotype column indicates mutations cited according to the old nomenclature (*rfa*), whereas genotypes in parentheses in the phenotype column are cited according to the new nomenclature (*waa*).

adhesive (Becton Dickinson Biosciences, Temse, Belgium) as previously described (30). Cultures and ε-PL stock solutions were prepared in MES buffer, and mixed to yield a final concentration of 5×10^5 CFU/ml plus 0, 1/2× MIC, MIC, or 2× MIC ε-PL. The samples were incubated 240 min at 25°C before the cells were harvested by centrifugation (5,000 × *g*, 10 min), washed three times, and resuspended in MES buffer. The suspension was added to the Cell-TAK-coated coverslip, incubated 15 min at room temperature, and rinsed with MES buffer. The coverslip with immobilized cells was briefly air dried and mounted in a JPK Biocell (JPK Instruments, Berlin, Germany).

Intermittent contact mode AFM images were recorded in air with a JPK NanoWizard II AFM (JPK Instruments, Berlin, Germany) using silicon cantilevers (f = 300 kHz, k = 42 N/m; OMCL-AC160TS; Olympus, Mannheim, Germany). Prior to imaging, the cantilever tip was cleaned by UV-ozone treatment for 40 min. AFM images were recorded at 512 pixels per line at a scan rate of 0.5 Hz and an area of 4 by 4 μm for *E. coli* and 3 by 3 μm for *L. innocua* cells. Images of at least three different cells were recorded from each sample, and all samples were prepared in triplicate. AFM images were processed in JPK Data Processing software (v4.2.50) by subtraction of a first-order polynomial fit from each scan line, except from areas containing important structures. Isolated scan lines with noise were removed from images, and omitted lines were reconstructed using average values of adjacent lines.

The effects of ε-PL on the cell structure and on the outer and inner membranes of *E. coli* and *L. innocua* cells were investigated by transmission electron microscopy (TEM). Samples were prepared by mixing the bacterial suspension, ε-PL, and MES-buffer to a final concentration of 5×10^5 CFU/ml plus 0, 1/2× MIC, MIC, or 2× MIC of ε-PL. Samples were incubated for 4 h at 25°C, and the cells were harvested by centrifugation (5,000 × *g*, 10 min), washed once in MES buffer, and washed three times in fixation buffer (2% glutaraldehyde in 0.1 M cacodylate buffer [pH 6.0]) before resuspension in fixation buffer and incubation for 3 days at 4°C. The cells were then washed three times in 0.1 M cacodylate buffer at pH 6.8 and 7.2 and postfixed in 1% osmium tetroxide in 0.1 M cacodylate buffer at pH 7.2 for an hour. The cells were washed twice with 0.1 M cacodylate buffer at pH 7.2 and twice with 0.05 M maleate buffer at pH 5.2. The samples were postfixed with 0.5% uranyl acetate in 0.05 M maleate buffer for an hour and then washed twice with 0.05 M maleate buffer at pH 5.2, followed by several dehydration steps using increasing ethanol concentrations (70%, two times for 10 min each time; 90%, two times for 10 min each time; 96%, two times for 10 min each time, and 99%, two times for 15 min each time), and washed with propylene oxide for two times for 15 min each time. Pellets were infiltrated with a 1:1 mix of propylene oxide and Epon (TAAB 812; TAAB Laboratories, Berks, England) overnight and then with pure Epon for 8 h. Fresh Epon was used for embedding, which was performed by using polymerization for 48 h at 60°C. The Epon blocks were trimmed, and a 1-μm section was colored with 1% toluidine blue to get an overall view of the pellet from which a representative area was selected for ultrathin sectioning. Ultrathin sections (40 to 50 nm) were made using an Ultramikrotom Leica Ultracut UCT (Leica Microsystems, Vienna, Austria) with a 45° diamond knife from Diatome (Biel, Switzerland). Sections were placed on a 300-mesh Formvar-carbon-coated nickel grid, contrasted for 10 min in saturated uranyl acetate (31), rinsed with about 25 droplets of water, dried, further contrasted with lead citrate (32) for 2 min, washed with about 10 droplets of water, and finally dried. The cells were observed by using a Phillips CM 100 transmission electron microscope (FEI, Eindhoven, The Netherlands) operated at 80 kV, and images were recorded with a Megaview III charge-coupled device camera (Olympus SIS, Münster, Germany).

(ii) Effect on cell membrane integrity studied on whole cells. ε-PL's effect on membrane integrity was evaluated by staining with the membrane-impermeant DNA binding stain propidium iodide (PI). Two different PI dyes were used for *E. coli* and *L. innocua*. We prepared a 4× PI work solution (kit L13152) and a 1.5 mM PI work solution (kit L7012) according to the manufacturer's instructions for *E. coli* and *L. innocua* staining, respectively. Stains were stored in the dark at −20°C until use. Untreated cells and heat-killed cells (30 min, 85°C) were used to identify PI-negative (live) and PI-positive (dead) cells, respectively. Heat-killed cells and 5×10^5 CFU/ml portions of cells treated with a final ε-PL concentration of 0, 1/2× MIC, MIC, and 2× MIC in TSB for 4 h at 25°C were harvested by centrifugation (5,000 × *g*, 10 min), and the pellets were resuspended in 200 μl of TSB into which 66 μl of 4× PI stain was added for *E. coli* or 2 μl of 1.5 mM PI stock was added for *L. innocua*. Stained samples were incubated in the dark for 15 min at room temperature and then analyzed by flow cytometry.

Flow cytometric analysis was performed using a Gallios (Beckman Coulter, Miami, FL) flow cytometer equipped with a 488-nm laser. Red fluorescence from PI-stained cells was collected in channels FL2 (575/26 nm) and FL3 (620/30 nm). Channels were calibrated with FlowCheck Fluorospheres (Beckman Coulter) before each experiment. Controls and samples were prepared in triplicate, and at least 30,000 events were collected for each sample, with a detection rate between 100 to 500 cells/s. Flow cytometry data were analyzed using Kaluza software (v1.2). Peaks of bacterial populations were gated based on their scattering in the forward and side directions to minimize noise. The gated populations were analyzed by dividing the negative and positive fluorescence signal histograms based on the signal positions of untreated and heat-killed cells, respectively. Statistically significant differences ($P < 0.05$) between the means of several groups was assessed by using one-way analysis of variance in Minitab 16.2.3 (Minitab, Inc., State College, PA).

Effect on cell membrane integrity studied on lipid vesicles. Three lipid compositions—DOPG, DOPC, or *E. coli* polar lipid extract (67% phosphatidylethanolamine, 23.2% phosphatidylglycerol [PG], 9.8% cardiolipin)—were used to form large unilamellar vesicles (LUVs).

LUVs were composed of DOPG, DOPC, or *E. coli* polar lipid extract. The organic solvent from the *E. coli* polar lipid was removed under N_2 gas, and the resulting lipid film was placed under vacuum in a desiccator to remove organic solvent traces. The vacuum was liberated and N_2 was applied to the glass vial containing the lipid film. The DOPG and DOPC powders were weighed off into glass vials. Lipids were hydrated in 70 mM calcein solution prepared in MES buffer to a lipid concentration of 10 mg/ml. The calcein-lipid solutions were shaken at 25°C (40°C for *E. coli* polar lipid extract) until lipid films were dissolved. Then, eight freeze-thaw cycles were performed using liquid nitrogen and a 25°C (or 40°C for the *E. coli* polar lipid extract) water bath. The suspensions were extruded through polycarbonate filters (100-nm-pore-size filter, 19 mm in diameter; Nuclepore Track-Etched membranes; Whatman, Clifton, NJ) 24 times using an Avanti mini-extruder preheated to 37°C. The vesicle solution was run over a PD-10 desalting column (GE Healthcare, Uppsala, Sweden) preequilibrated in MES buffer to remove untrapped calcein. The calcein-LUV-containing fraction was collected and diluted to a final lipid concentration of 55 μM. Calcein dye leakage was monitored by using a Tecan GENios Pro microtiter plate reader (Tecan Group, Männedorf, Switzerland) and 96-well black Nunc optical-bottom microtiter plates (catalog no. 265301; Thermo Scientific, Rochester, NY). A 200-μl aliquot of calcein-LUV solution was added to all wells, followed by measurement of the calcein fluorescence baseline (F_0) using excitation at 448 nm and detection at 485 nm at 37°C until the signals were constant. Then, ε-PL was added to a final concentration ranging between 0.00001 and 0.1 mg of ε-PL/ml in duplicate for DOPC and DOPG vesicles and ranging between 0.00001 and 0.05 mg of ε-PL/ml in duplicate for *E. coli* lipid vesicles. We included, as controls, untreated vesicles, vesicles treated with dextrin at concentrations equal to the highest ε-PL concentration, and free calcein without vesicles exposed to ε-PL. Microtiter plates were incubated 1 h at 25°C (37°C for *E. coli* polar lipid extract), followed by measurement of the calcein signal (F). The maximum fluorescence signal (F_{max}) was measured after rupture of all vesicles by adding 5 μl of 1% Triton X-100 solution to each well. We averaged the relative amount of released calcein calculated as follows: % calcein release = $[(F - F_0)/(F_{max} - F_0)] \times 100$. The baseline

was subtracted from all data points by using an average value of a linear section of each graph from at least 10 different concentrations.

Initial interaction of ε-PL with membranes using giant unilamellar vesicles. Giant unilamellar vesicles (GUVs) were prepared by using the electroformation method (33) in a home-built electroformation chamber as previously described (25). A mix of DOPG and DOPC in 20:80 ratios was dissolved in chloroform to a 10-mg/ml solution. For monolabeled GUVs, the lipid tracer DiO was added to the lipid-chloroform solution to a final concentration of 0.5% of the total lipid content, and a subsequent procedure without Alexa Fluor 488 and Alexa Fluor 633 was followed. For double-stained GUVs, a 15-μl aliquot of lipid solution was deposited on each platinum electrode in the electroformation chamber. Gentle application of N_2 gas into the chamber, followed by incubation at 95°C for 5 min, ensured the removal of organic solvent traces. The chamber was filled with 200 mM sucrose solution containing Alexa Fluor 488-labeled dextran and Alexa Fluor 633 hydrazide in a 1:1 mix. Platinum electrodes were connected to a function generator (Digimess FG100; Grundig Instruments, Nürnberg, Germany), and GUVs were formed by application of an alternating current with a 10-Hz sinusoidal wave function and amplitude of 1.5 V for 90 min in the dark at room temperature. GUVs were removed from the platinum electrodes by gently mixing the GUV suspension in the chamber. The GUV solution was run over a PD-10 desalting column previously equilibrated in 200 mM glucose. Eluent containing GUVs were collected in an eight-chambered borosilicate cover glass (catalog no. 155411; Nunc Lab-Tek). Glucose solution was added to each chamber, and the GUV solution was left overnight at 4°C to allow the sedimentation of GUVs to the bottom of the cover glass.

We visualized the interaction between ε-PL and GUVs by using an LSM 700 (Zeiss, Göttingen, Germany) with a Plan-Apochromat 40×/1.3 oil immersion objective lens at room temperature. Excitations of DiO, Alexa 488, and Alexa 633 were performed at 488, 488, and 639 nm, respectively, and fluorescence emissions were collected using a SP 640 filter for DiO and Alexa 488 and using a LP 640 filter for Alexa 633 with a dichroic beam splitter at 629 nm. Five microliters of 5-mg/ml ε-PL solution dissolved in MES buffer was added to the GUV solution in the opposite corner of focus, and imaging was initiated. A time series of images of the same field of view was taken sequentially every 4 s, with a pixel dwell of 0.79 μs and an image size of 1,024 lines per frame, where each line was averaged twice. No changes to the GUVs were observed in the first 10 to 20 min after addition of ε-PL due to slow diffusion of molecules in the glucose suspension.

Visualizing the interaction between ε-PL and its target. (i) Interaction with cells visualized by fluorescence microscopy. We assessed the interaction between bacterial cells and ε-PL using confocal laser scanning microscopy (CLSM) and FITC-labeled ε-PL. Triplicate bacterial suspensions of *E. coli* and *L. innocua* were prepared in MES buffer at a density of 10^7 CFU/ml. Each bacterial suspension was mixed with a 5,000-mg/liter stock solution of FITC-labeled ε-PL to a final concentration equal to 2× MIC against the respective model organism. Samples were kept in the dark for an hour at 25°C and then visualized by using a Zeiss LSM 700 with Plan-Apochromat 40×/1.3 and 100×/1.45 oil immersion objective lenses and a 488-nm laser. Images of random areas were recorded, and at least 100 cells per replica were imaged.

(ii) Interaction with supported lipid bilayers visualized by AFM. Small unilamellar vesicles (SUVs) were prepared with *E. coli* polar lipid extract and used to form supported lipid bilayers. A vesicle solution was prepared as for calcein-encapsulated vesicles and subjected to freeze-thaw cycles. To obtain SUVs, the vesicle solution was sonicated (3-mm probe, 70 W, 50% of maximal power; Sonopuls ultrasonic homogenizers; Bandelin Electronic, Berlin, Germany) until clear while immersed in an ice bath. Supported lipid bilayers were formed on freshly cleaved mica squares (10 mm^2) glued to 18-mm circular coverslips by mixing SUV solution and $CaCl_2$ in MES buffer to final concentrations of 0.3 mg of lipid/ml and 20 mM, respectively. Membranes were formed on the mica substrate during a 20-min incubation at 37°C in a temperature-controlled JPK Biocell (JPK Instruments, Berlin, Germany). Excess SUVs were removed in a washing procedure using MES buffer without $CaCl_2$, and the supported lipid bilayer was kept in MES buffer at 37°C for the reminder of the experiment. AFM imaging was performed in contact mode using CSC38/noAl cantilevers (Mikromash, Tallin, Estonia; k = 0.03 to 0.09 N/m). Images of supported lipid bilayers were acquired before and after a 60-min incubation with ε-PL. The supported lipid bilayer was washed five times in MES buffer before images of at least three random areas were acquired on each of triplicate samples. All images were of 5-by-5-μm areas and recorded at 512 pixels per line and a scan rate of 0.5 Hz.

RESULTS AND DISCUSSION

ε-PL affects the cell morphology and membrane integrity of *E. coli* more severely than it affects *L. innocua*. We assessed the antimicrobial activity of ε-PL by monitoring its inhibitory effect on growth and cell viability of *E. coli* and *L. innocua*. The MIC was 74 mg/liter for *E. coli* and 750 mg/liter for *L. innocua*. The MIC for *E. coli* was similar to previous reports (3, 8, 10), while we found somewhat higher MICs for *L. innocua* compared to previous studies that used the taxonomically similar *L. monocytogenes* (4, 34).

Incubation with ε-PL at the MIC showed a biocidal activity leading to 2 to 3 log decrease in CFU (Fig. 1). Increasing the ε-PL concentration to 2× MIC resulted in a faster biocidal effect, and no CFU could be detected after 8 h of incubation, demonstrating a >5.5-log reduction. It therefore appears that growth inhibition is directly related to loss of viability. Interestingly, the biocidal effect at 1/2× MIC was only temporary, and growth resumed after approximately 15 h of incubation (Fig. 1). Hence, the ε-PL was either degraded or deactivated (e.g., by adsorption), allowing the surviving cells to grow.

We hypothesized that the primary target of ε-PL is the cell membrane and therefore quantified the dose-dependent effect on membrane integrity by using PI staining combined with flow cytometry. Increasing concentrations of ε-PL caused permeabilization of both *E. coli* and *L. innocua* cells in a dose-dependent manner (Fig. 2). At the MIC, the number of *E. coli* cells with a compromised membrane was not significantly different from the control sample with heat-killed cells. The effect on membrane permeability in *L. innocua* was, however, less pronounced. Even at 2× MIC, the number of cells with a compromised membrane was lower than the control sample with heat-killed cells, demonstrating that ca. 30% of *L. innocua* cells retained an intact membrane despite exposure to ε-PL at concentrations that lead to a 4-log reduction in the number of viable cells (Fig. 1). Although the membrane may be the primary target, this result indicates that ε-PL interacts with other targets that lead to cell death in *L. innocua*, even when cell membrane integrity is maintained.

We examined morphological effects of ε-PL on *E. coli* and *L. innocua* by AFM and TEM imaging. ε-PL exposure resulted in severe morphological changes of *E. coli* cells, indicating partial removal of the outer membrane, indentations in the cell wall, and patchy changes to the cell stiffness, as shown in AFM amplitude and phase images (Fig. 3). TEM images of cross sections confirmed these observations. Exposure to 2× MIC led to complete disintegration of the cells, whereas lower concentrations resulted in removal of the LPS layer, which protruded as vesicles from cell surface (Fig. 4). Such protrusions of membrane or LPS binding to ε-PL bound were also observed by optical microscopy of *E. coli* incubated with fluorescently labeled ε-PL (Fig. 5A). The optical images also indicated that ε-PL entered *E. coli* and *L. innocua* cells,

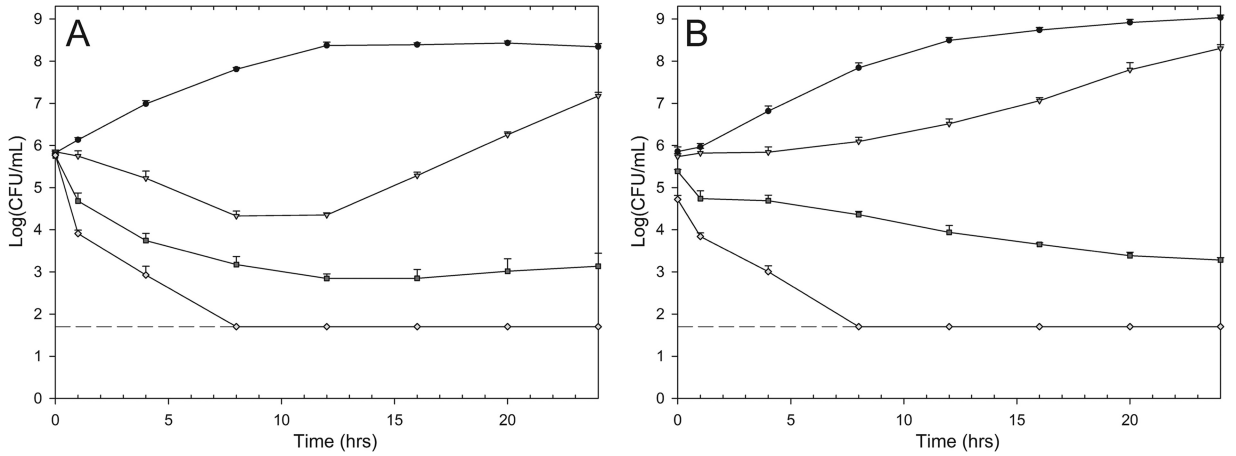

FIG 1 Number of viable *E. coli* (A) and *L. innocua* (B) cells during treatment with ε-PL at 0 (black circles), 1/2× MIC (gray triangles), MIC (dark gray squares), and 2× MIC (white diamonds) in TSB (pH 6.0) at 25°C. A dashed line indicates the detection limit: 50 CFU/ml. Error bars indicate the standard deviations (SD) ($n = 3$).

thereby supporting that ε-PL have intracellular targets (Fig. 5), as previously proposed (35).

Despite the documented effect on cell membrane integrity, we did not observe severe morphological changes for ε-PL-treated *L. innocua* cells, presumably because the peptidoglycan maintained the cell structure (Fig. 3, 4, and 5). Only TEM images indicated changes to the cell membrane, which appeared to partly disassociate from the cell wall (Fig. 4H, white arrow).

Antimicrobial activity of ε-PL relies on electrostatic interactions. We hypothesized that ε-PL's interaction with the cell surface is based on electrostatic forces and would be affected by the presence of other positively charged molecules that compete for negatively charged sites on the cell surface. We tested this hypothesis by measuring the MIC in the presence of various Mg^{2+} and Ca^{2+} concentrations. Indeed, the presence of divalent cations reduced the antimicrobial effect of ε-PL in a dose-dependent manner, and the effect of ε-PL could be completely reversed by cations in the media (Fig. 6). Because LPS in the outer membrane are polyanionic, they need cations to sustain the lateral interaction of lipids, and the fluidity and melting of the membrane is affected when the cationic homeostasis is disturbed (18, 36). The effect of ε-PL on Gram-negative bacteria could therefore be due to the direct effect from interacting with ε-PL, but it is also possible that there is an indirect effect through depletion of Mg^{2+} and Ca^{2+} from the LPS due to ε-PL occupying their interaction sites.

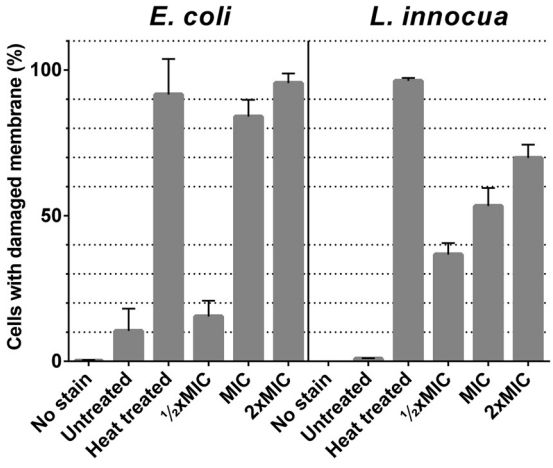

FIG 2 Membrane damage of heat-treated at 85°C or live cells of *E. coli* (left) and *L. innocua* (right) treated with or without ε-PL for 4 h in TSB (pH 6.0) at 25°C. The cells were harvested and resuspended in TSB before PI staining, except for the control without stain. The cells with compromised membranes were stained with PI. Error bars indicate the SD ($n = 3$).

ε-PL interacts with phosphate groups in the inner core of the LPS. Interaction of ε-PL by electrostatic forces implies that interactions with negatively charged groups in the cell wall, membrane, or LPS are critical for the antimicrobial action of ε-PL. Indeed, ε-PL has previously been proposed to remove LPS (3), which acts as the initial barrier for polycationic peptides in their attempt to reach their main site of action, namely, the cell membrane (16, 37). However, the molecular interaction between ε-PL and different parts of LPS has not been investigated before. We hypothesized that ε-PL competes with divalent cations for binding to the phosphate groups in the LPS inner core and causes removal of the outer membrane of Gram-negative bacteria. We tested this hypothesis by measuring ε-PL adsorption and determining the MIC for a range *E. coli* strains with mutations that change the composition of the cell exterior.

The hypersensitive deep-rough LPS mutants normally have decreased MICs compared to the wild type when treated with, e.g., hydrophobic antibiotics, anionic detergents, or other cationic peptides (18, 36, 38–40), but for ε-PL the MIC was higher in all of the deep-rough LPS mutants, which have no phosphoryl groups in the LPS inner core, making the exterior more hydrophobic. We propose that ε-PL's interaction with phosphate groups on heptose (Hep) I and II in the inner core of the LPS is particularly important. The sequence of enzymatic events that accumulate phosphate groups on the LPS is as follows: WaaG catalyzes glucosylation of Hep II, which increases the substrate specificity of the enzymes WaaP and WaaY (39). WaaP adds a phosphoryl substituent to Hep I, which is required for WaaQ to bind Hep III to Hep II. This event is followed by the addition of a phosphate group to Hep II, catalyzed by WaaY (38, 39). Deletions in the genes *waaC*, *waaF*, *waaG*, *waaP*, *waaY*, *waaP*, and *waaQ* lead to removal or

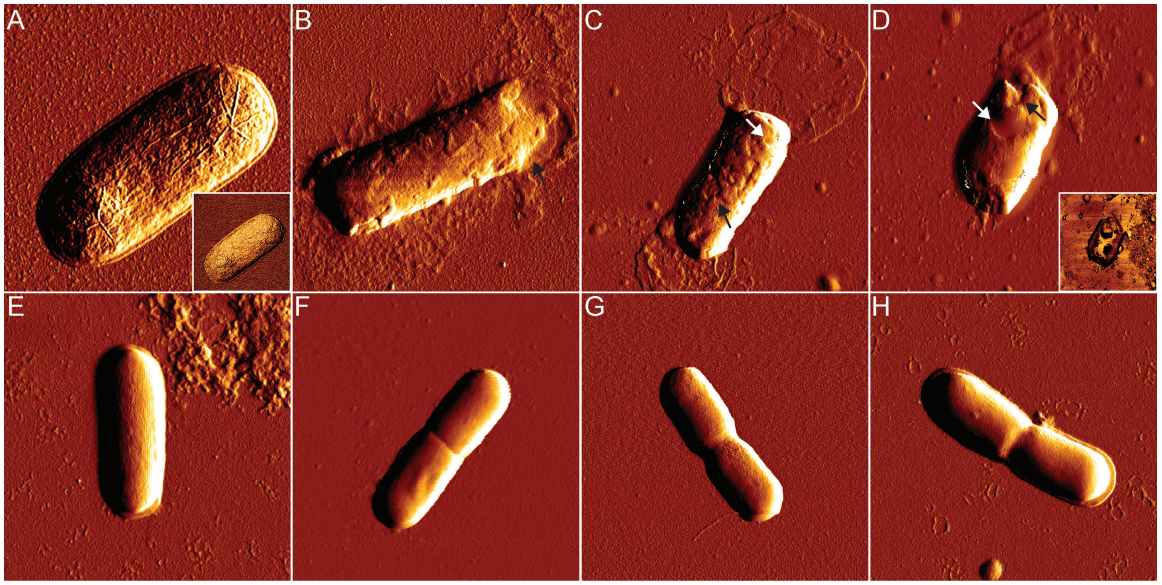

FIG 3 AFM amplitude images of *E. coli* (A to D) and *L. innocua* (E to H) cells recorded in air after treatment with ε-PL at 0 (A and E), 1/2× MIC (B and F), MIC (C and G), or 2× MIC (D and H) in MES buffer (pH 6.0) for 4 h at 25°C. Insets show phase images of same area as the corresponding amplitude images, where bright and dark areas indicate soft/sticky or stiff surfaces, respectively. Black arrows indicate visible areas of structural changes in the form of indentations in the cell wall, while white arrows point to areas indicative of the removed LPS layer. The images of *E. coli* and *L. innocua* show areas of 4 by 4 μm and 3 by 3 μm, respectively.

dephosphorylation of Hep I and/or II, and MIC was higher for these strains compared to the parent strain (Table 1). The strains with mutations to both Hep I and Hep II (Δ*waaC* and Δ*waaP* mutants) furthermore exhibited a substantial decrease in ε-PL adsorption, as indicated by an only moderate change in zeta potential when ε-PL was added to cells suspended in MES buffer (Table 1). The smaller increase in zeta potential during ε-PL exposure of the Δ*waaC* and Δ*waaP* mutants compared to the other deletion mutants could either indicate a weaker binding of the positively charged ε-PL or less removal of the negatively charged LPS layer in these mutants.

In addition to the effects from changes to the LPS structure, we also found an increased tolerance to ε-PL in the Δ*rscC* mutant, which overexpresses the capsular exopolysaccharide colanic acid (Table 1). Colanic acid helps to regulate the three-dimensional structure of *E. coli* biofilms (41) and functions as a protective barrier (42). We therefore propose that the colanic acid chelates ε-PL and thereby increases the tolerance of the *rscC* mutant by preventing or delaying its access to the inner and outer membranes.

Interaction of ε-PL with phospholipid bilayers results in the formation of vesicles and micelles. In addition to the obvious effect on the outer membrane of Gram-negative bacteria, we expected the site of action for ε-PL to be the plasma membrane because cationic antimicrobial peptides generally act as membrane permeabilizers, membrane thinners, or micellization agents

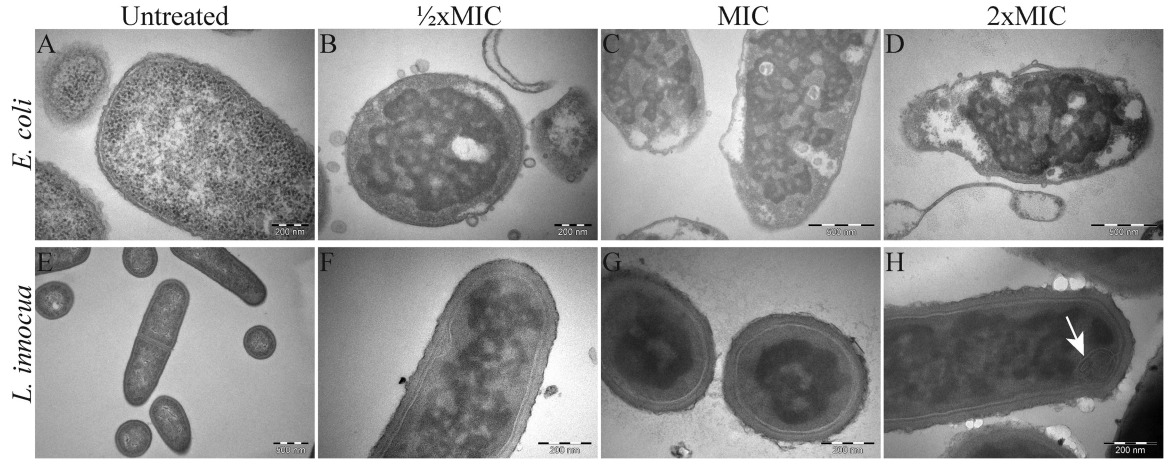

FIG 4 Representative TEM images of *E. coli* (A to D) and *L. innocua* (E to H) cells treated with ε-PL at 0 (A and E), 1/2× MIC (B and F), MIC (C and G), or 2× MIC (D and H) in MES buffer (pH = 6.0) at 25 C° for 4 h. White arrow indicates intracellular membrane damages caused by ε-PL treatment. Magnifications: ×64,000 (A and B), ×46,000 (C and D), ×25,000 (E), and ×92,000 (F, G, and H).

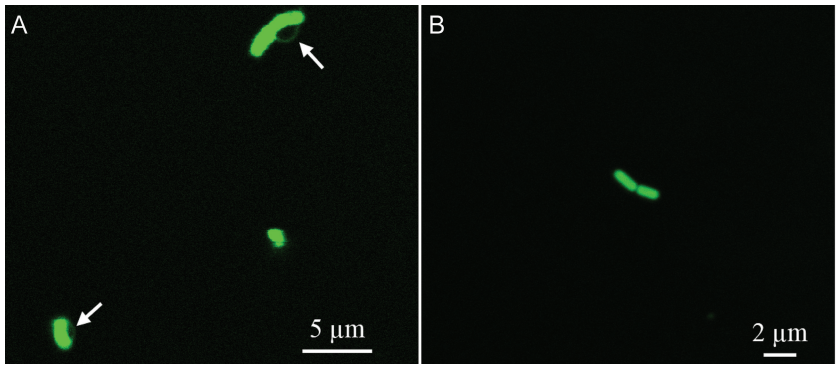

FIG 5 Representative CLSM images of *E. coli* (A) and *L. innocua* (B) cells treated an hour with FITC-labeled ε-PL at 2× MIC in MES buffer (pH 6.0) at 25°C. White arrows indicate the protruding LPS layer caused by ε-PL treatment.

in a detergent-like way through different mechanisms (3, 19, 23). To obtain a more detailed understanding of the interaction of ε-PL with the plasma membrane, we studied the effect of ε-PL on model membranes prepared as large or giant unilamellar vesicles (LUV and GUV) in suspension, or as supported lipid bilayers on a mica surface. These model systems allowed investigation of how the composition of the lipid head group affected the interaction of ε-PL with the membrane. We compared the effect of ε-PL on vesicles formed by *E. coli* polar lipid extract (mimicking the natural interaction between ε-PL and the cytoplasmic membrane) and vesicles prepared from the negatively charged DOPG, the zwitterionic DOPC, or a mixture of the two. We used DOPC and DOPG due to their low melting points, charges, and simplicity. Integrity of the vesicles upon exposure to ε-PL was evaluated based on the release of calcein from LUVs and by visualization of fluorescently labeled GUVs by CLSM.

The negatively charged DOPG vesicles became permeabilized at lower ε-PL concentrations than vesicles prepared from *E. coli* lipids or the neutrally charged DOPC, as shown by release of calcein from the vesicles (Fig. 7). Interestingly, calcein release leveled off at 20% release when DOPG vesicles were exposed to increasing concentrations of ε-PL (Fig. 7). We interpret this observation to mean that ε-PL binding was not accompanied by large changes in membrane organization (despite the higher affinity of ε-PL for DOPG than for DOPC) and thereby only released a fraction of the encapsulated calcein. Furthermore, we observed that ε-PL interacted with free-calcein at concentrations above 0.002 mg/ml ε-PL (data not shown), resulting in a markedly decreased fluorescence signal from calcein above a 0.004-mg/ml ε-PL concentration. We conclude that ε-PL interacted with negatively charged phospholipids and, to a lesser extent, with zwitterionic phospholipids.

To confirm the indication that ε-PL permeabilized membranes and to visualize the peptide-lipid interaction in solution, we used

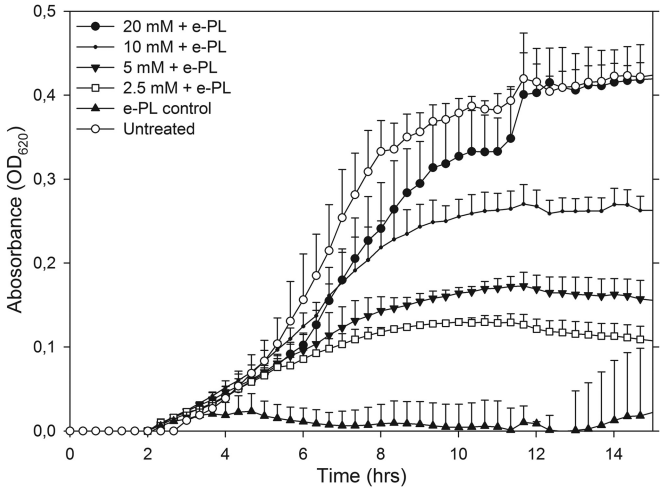

FIG 6 Growth inhibition profile of *E. coli* cells exposed to either no ε-PL (white circles) or ε-PL at MIC, together with increasing concentrations of Mg^{2+} and Ca^{2+}, both in final concentrations of 0 mM (black triangles), 2.5 mM (white squares), 5 mM (black inverted triangles), 10 mM (black dots), or 20 mM (black circles) in TSB (pH = 6.0) at 25°C. Error bars indicate the SD ($n = 3$). The growth profiles for *E. coli* with different divalent cation concentrations but no ε-PL are not shown since they matched those of the untreated cells.

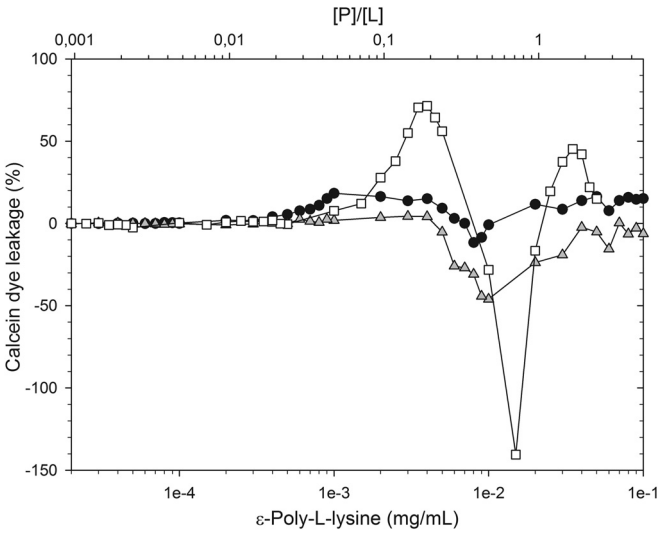

FIG 7 Membrane permeabilization by ε-PL monitored as determined by measuring the leakage of calcein dye from vesicles made of DOPG (black circles), DOPC (gray triangles), or *E. coli* polar lipid extract (white squares) in MES buffer as a function of the peptide/lipid concentration ([P]/[L], upper axis) or of the peptide concentration (lower axis). The calcein intensity signal from the released dye was monitored before and after ε-PL treatment for an hour at 25°C (37°C for *E. coli* lipid) and normalized to the signal obtained at full permeabilization for the individual [P]/[L] ratios. A lipid concentration of ~11 nmol was used for all [P]/[L] ratios.

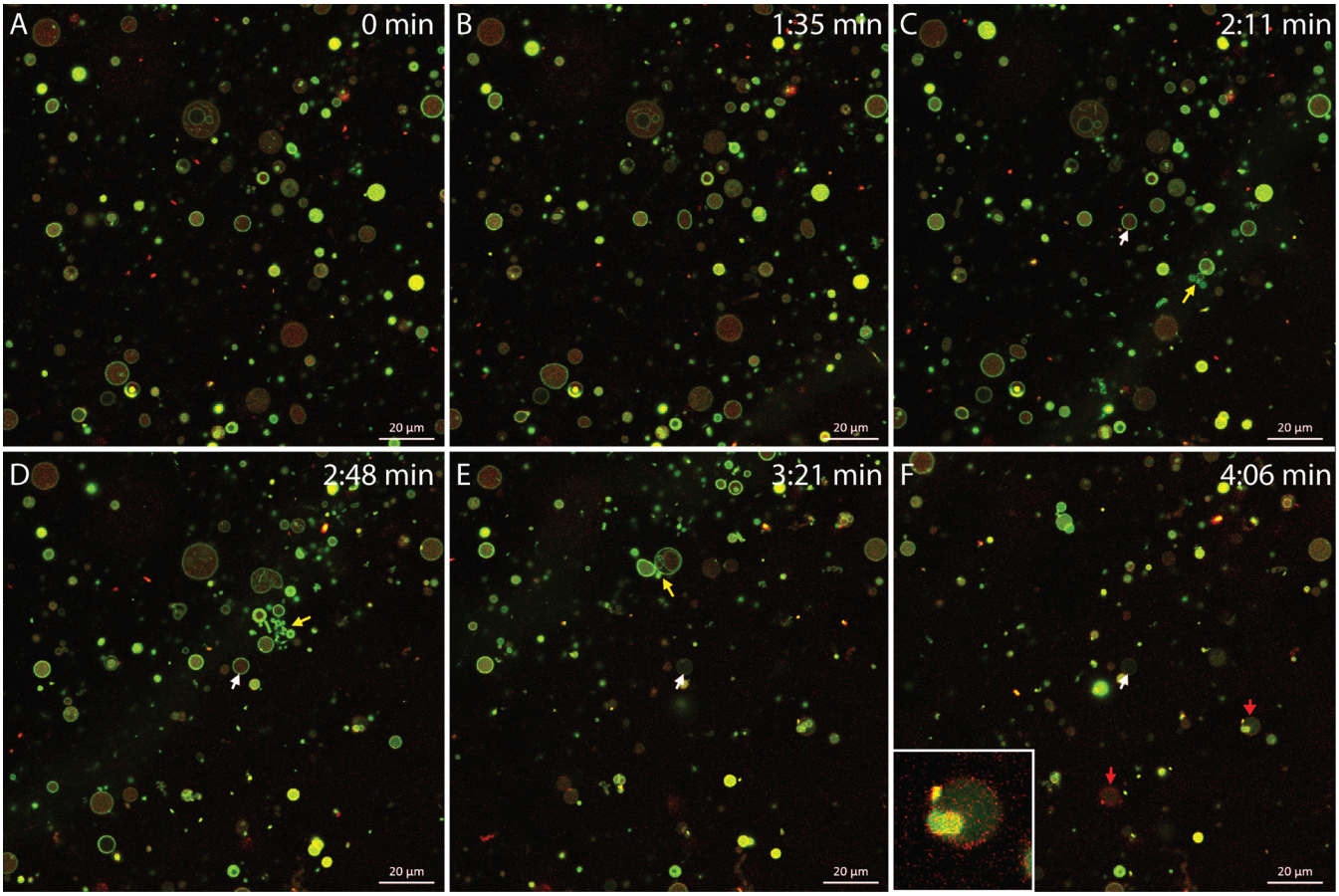

FIG 8 CLSM time series of ε-PL's initial interaction at room temperature with GUVs composed of DOPG:DOPC (20:80) and stained with the membrane-bound dye Alexa 488 dextran (green) and intravesicular with the water-soluble Alexa Fluor 633 hydrazide (red). Untreated GUVs (A) remained intact and within the same field of view until the onset of the ε-PL "wave front" from the lower right corner (B). Progression of ε-PL to the upper left corner (B to F) results in three distinct interactions between ε-PL and GUVs: a nonlytic decrease in fluorescence intensity (white arrows), vesiculation of GUVs (yellow arrows), and inversion of dye position (red arrows, and inset in panel F). Bars, 20 μm.

GUVs with a 20:80 ratio of DOPC to DOPG stained with either DiO or fluorescently labeled dextran or hydrazide. DiO (blue in Video S1 in the supplemental material) is a lipophilic tracer that incorporates into the hydrophobic region of membranes and becomes highly fluorescent. Dextrans are anionic hydrophilic polysaccharides that will associate with the membrane of GUVs, whereas hydrazide is a dissolved membrane-impermeant compound situated in the center of GUVs. Introducing ε-PL to hydrazide-filled (red) GUVs stained with Alexa Fluor 488-labeled dextrans (green) leads to bursting or permeabilization of GUVs, releasing the red fluorescence from the vesicles' interior within minutes of exposure (Fig. 8). The treatment did not rupture all GUVs, and the remaining GUVs had large and strongly fluorescent "membrane-buddings" protruding from the surface (see Video S1). Time-lapse imaging revealed further details. First, a nonlytic reaction happened for a small subset of GUVs where the fluorescence intensity from the membrane-bound dye decreased with a concomitant release of hydrazide from the vesicle (Fig. 8C to F, white arrows; see also Video S2 in the supplemental material). Second, some GUVs transformed into smaller vesicles and formed aggregates (Fig. 8C to E, yellow arrows). Lastly, some GUVs inversed the dyes, so that the dye within GUVs was positioned on the exterior of GUVs, which could happen if ε-PL adsorbed to the GUV surface and also interacted with the dye (Fig. 8F, red arrows).

The effect of ε-PL at subpermeabilization concentrations on supported lipid bilayers could be visualized using AFM and hence help to elucidate how ε-PL act on membranes at the initial stage of treatment. To achieve nanometric resolution imaging of ε-PL interacting with a membrane under physiological conditions, we imaged supported lipid bilayers of *E. coli* lipid by AFM in MES buffer before and after exposure to ε-PL. Untreated bilayers appeared as a continuous and homogenous bilayer of liquid-disordered (L_d) lipid phase. The height of the bilayer was approximately 3 to 3.5 nm (data not shown) and contained a few round structures protruding ~0.6 nm from the bilayer (Fig. 9A and D). Imaging of the bilayers after exposure to ε-PL at 0.0005 mg/ml (i.e., 148 times less than the MIC) for 1 h revealed numerous round structures protruding 1 to 2 nm from the L_d lipid phase and indentations of ~200-nm width and 0.5-nm depth (Fig. 9B and E). Exposure to ε-PL at 0.003 mg/ml (i.e., 25 times less than the MIC) led to extensive damage to the bilayer, seen as round or worm-like holes in the layer (Fig. 9C and F). Similar worm-like structures protruding from the surface of the bilayer were also observed. We propose that these structures are ε-PL interacting with the bilayer, which strips off phospholipids to cause the ap-

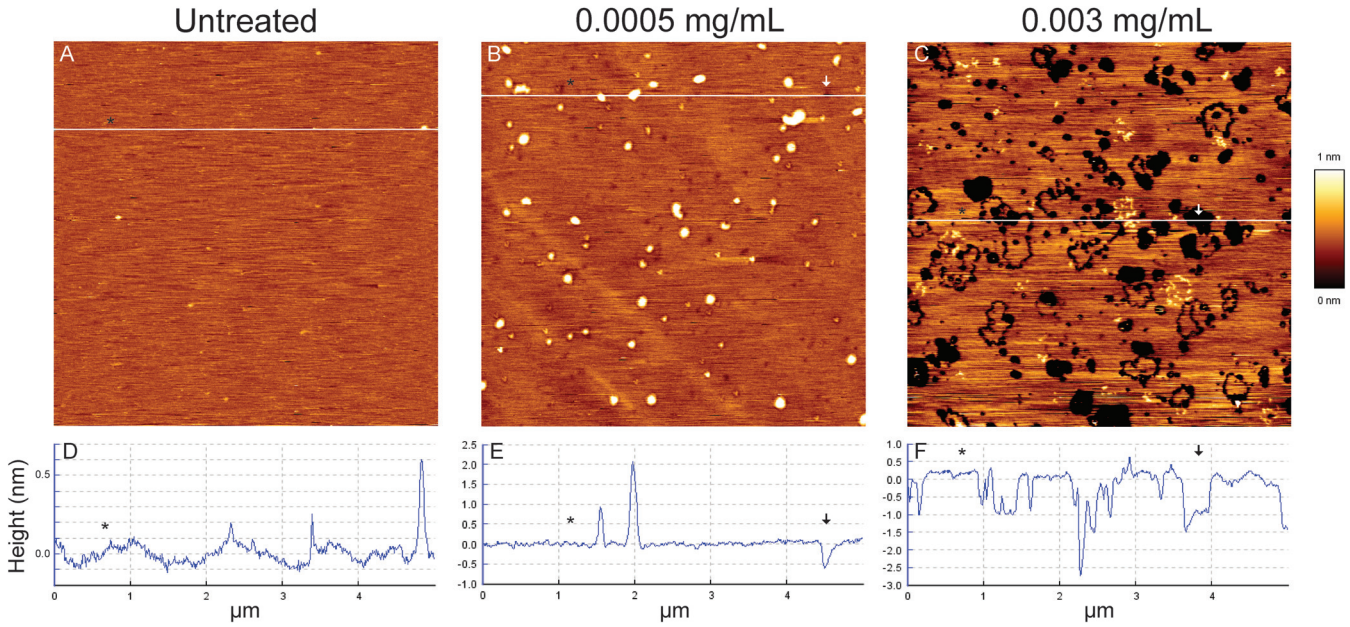

FIG 9 Contact-mode AFM height images of ε-PL's effect on supported lipid bilayers from *E. coli* recorded in MES buffer (pH 6.0) at 37°C. Representative images of untreated *E. coli* lipid (A) and ε-PL-treated supported lipid bilayers for 1 h at a final concentration corresponding to weak (B) and strong (C) effects on calcein leakage (see Fig. 6) are shown. The supported lipid bilayers were rinsed with MES buffer before imaging. Underneath each height image is a cross-sectional profile taken at the white line in the corresponding height image. The liquid disordered lipid phase and holes are exemplified by asterisks and arrows, respectively. Images are 5-by-5-μm sections, and the bright and dark areas correspond to higher and lower structures than the supported lipid bilayer mean height.

pearance of holes. The holes did not have the same depth as the height of the bilayer. Some were 1 to 1.5 nm, and others were 3 nm deep, indicating removal from either one or both bilayer leaflets (Fig. 9C and F). Visualization of ε-PL's interaction with the supported lipid bilayer thus supported our hypothesis that ε-PL interacts with the negatively charged head groups of phospholipids, which in turn results in the removal of phospholipids from either one or both layers of the membrane.

ε-PL has a carpet-like mechanism that causes disruption by imposing negative curvature. The ε-PL peptide is composed of hydrophilic residues, and cannot interact directly with the hydrophobic parts of membranes (43). ε-PL's mechanism of action is therefore most likely a nonspecific carpet-like mechanism. Our results support this mechanism, since ε-PL did not permeabilize the zwitterionic DOPC LUVs but only the negatively charged DOPG and *E. coli* LUVs (Fig. 7). Furthermore, ε-PL lead to detergent-like removal of LPS from whole cells (Fig. 4), the removal of phospholipids from supported lipid bilayers (Fig. 9C), and the bursting and concomitant formation of vesicles or micelles from GUVs (Fig. 8 and see Videos S1 and S2 in the supplemental material).

The ability of peptides to generate negative curvature in membranes is highly dependent on their content of lysine and arginine (44). We propose that ε-PL is positioned at the membrane surface, where it imposes a negative membrane curvature, as indicated by AFM (Fig. 9C) and fluorescence imaging (Fig. 5). This leads to peptide-induced micellization and/or vesiculation that disrupts membrane integrity and causes thinning of membranes in localized areas, which we observed by optical microscopy (Fig. 8), TEM (Fig. 4), and AFM (Fig. 9). Antimicrobial peptides with high lysine contents generate negative curvature in membranes by a specific peptide-lipid interaction, wherein the cationic amine group induces negative curvature wrapping of anionic membranes to form inverted hexagonal phases (44). The difference in peptide backbone structure by ε-PL from the general α-peptide could induce a different lipid phase than the proposed inverted hexagonal phases, but this is not known. We observed two distinct structural features of the supported lipid bilayer after exposure to a low concentration of ε-PL (Fig. 9B): (i) the protruding membrane structures, which could be lipid undergoing negative curvature wrapping by ε-PL, and (ii) indentations in the supported lipid bilayer, which could be regions undergoing membrane thinning due to the protrusion of lipid elsewhere. At higher ε-PL concentrations, the protruding lipid regions are removed as vesicles or micelles, as indicated by the removal of one or both leaflets of the supported lipid bilayer (Fig. 9C) and by the protrusion of vesicles from treated cells (Fig. 4).

In conclusion, we propose that ε-PL interacts with *E. coli* membranes through a carpet-like mechanism that forms vesicles or micelles by imposing negative curvature through its interaction with the phospholipid headgroups of the bacterial membrane (Fig. 10). Because ε-PL interacts more readily with negatively charged headgroups, it has a relatively low toxicity against mammalian cells (8) and yeast cells (3, 45), and differences in susceptibility among microorganisms could be caused by differences in membrane composition. For example, the membrane of *L. innocua* contains lysine-derivatized phosphatidylglycerol and lysylcardiolipin (19, 46, 47). The lysylcardiolipin is zwitterionic (46) and therefore has no net negative charge, while lysine-derivatized PG further reduces the negative charge of membrane diminishing its affinity for cationic peptides (19). These components the in cytoplasmic membrane of *L. innocua* could contribute to the higher MIC and lower degree of membrane permeabilization of *L. innocua* compared to *E. coli* cells. Differences in susceptibility can

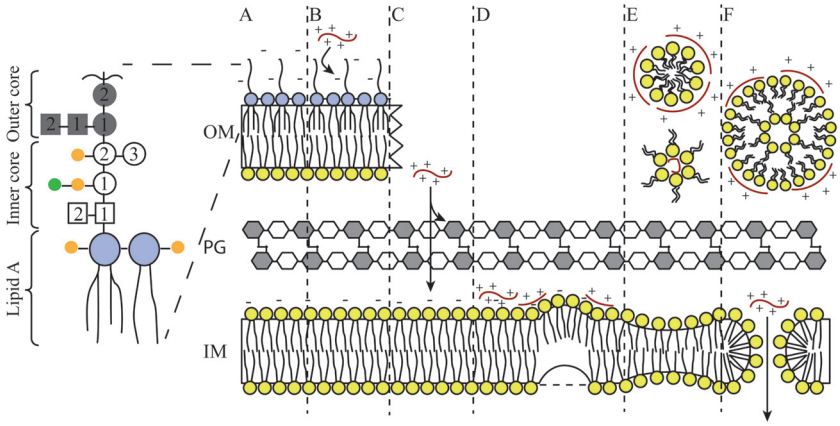

FIG 10 Schematic illustration of ε-PL's proposed mechanism of action on *E. coli* cells. (A) Untreated cell wall with intact outer membrane (OM), peptidoglycan layer (PG), and inner membrane (IM). The exterior leaflet of the outer membrane is made of lipopolysaccharides (LPS; the enlarged drawing to the left shows the LPS structure of *E. coli* BW25113), which consist of a phosphorylated D-glucosamine disaccharide (purple circle) with attached fatty acids, a polysaccharide with an inner and outer core, and an O-antigen (not shown here). The inner core is composed of ketodeoxyoctonate (Kdo; white squares) and L-glycero-D-manno-heptose (Hep; white circles) linked to phosphate groups (orange circles) and 2-aminoethyl phosphate (green circle). The outer core is build of D-glucose (Glc; gray circles) and D-galactose (gray squares). (B) Electrostatic forces guide the interaction between ε-PL (red molecule) and the LPS (purple headgroup), which ultimately removes the LPS layer in a detergent-like manner. ε-PL favors the electrostatic interaction with phosphate groups on Hep I and II of LPS, but they are not required for LPS removal. (C) ε-PL gains access to the periplasmatic space, and it is unknown whether ε-PL could interact with the peptidoglycan layer (*N*-acetylmuramic acid; gray hexagons, *N*-acetylglucosamine; white hexagons) or traverse through the peptidoglycan layer and interact electrostatically with the inner membrane, thereby initiating the nonspecific carpet-like mechanism. (D) When ε-PL reaches a threshold concentration on the inner membrane, it enforces the negative curvature of one (dashed line at lower leaflet) or both (solid line at lower leaflet) leaflets of the membrane. (E) When one membrane leaflet is removed by ε-PL, it causes thinning of the inner membrane, and the removed phospholipids (yellow headgroup) could form either inverse hexagonal or normal micelles, as illustrated. (F) If both leaflets of the inner membrane are removed by ε-PL, the removed phospholipids form vesicles and leave behind a hole in the inner membrane through which excess ε-PL can gain access to the cytoplasm and cause further damage to the cell.

also be caused by differences in the ability of ε-PL to access the membrane. The ability of ε-PL to remove the LPSs of Gram-negative bacteria enhances their access to the cytoplasmic membrane, since LPS normally provides a continuum of negative charge that protects the cell against different cationic antimicrobial peptides (48, 49).

Due to the electrostatic nature of the interaction, as well as differences in the ability of ε-PL to access the membrane, the effect of ε-PL can be competitively inhibited by cations in the surrounding liquid. From our results, it can furthermore be speculated that an increase in pH would decrease the positive charge of ε-PL and thus reduce the electrostatic interaction with cells with a concomitant reduction in antimicrobial activity. ε-PL is an interesting peptide with antimicrobial properties toward a broad spectrum of microorganisms caused by its very general mechanism of action, while it has low cytotoxic activity toward eukaryotic cells due to the intrinsic differences in the composition of the phospholipid head groups of eukaryotic and prokaryotic cell membranes.

ACKNOWLEDGMENTS

We acknowledge financial support from the Danish Ministry of Higher Education and Science. B.S.V. and D.E.O. are supported by the Danish Research Foundation (inSPIN). M.S. is supported by iNANO and the Sino-Danish Center for Education and Research (SDC).

We thank Andrew Mark Louw for assistance with the flow cytometer and Karen Thomsen for postfixation, embedding, and TEM imaging of cells.

REFERENCES

1. **Russell NJ, Gould GW.** 2003. Major, new, and emerging food-poisoning and food-spoilage microorganisms, p 1–13. *In* Food preservatives. Kluwer Academic/Plenum Publishers, Dordrecht, Netherlands.
2. **Baird-Parker TC.** 2000. The production of microbiologically safe and stable foods, p 3–18. *In* Lund B, Baird-Parker TC, Gould GW (ed), Microbiological safety and quality of food. Springer-Verlag, Berlin, Germany.
3. **Shima S.** 1984. Antimicrobial action of ε-poly-L-lysine. J. Antibiot. **37:** 1449. http://dx.doi.org/10.7164/antibiotics.37.1449.
4. **Brandt AL, Castillo A, Harris KB, Keeton JT, Hardin MD, Taylor TM.** 2010. Inhibition of *Listeria monocytogenes* by food antimicrobials applied singly and in combination. J. Food Sci. **75:**M557–M563. http://dx.doi.org/10.1111/j.1750-3841.2010.01843.x.
5. **Geornaras I, Sofos JN.** 2005. Activity of ε-polylysine against *Escherichia coli* O157:H7, *Salmonella* Typhimurium, and *Listeria monocytogenes*. J. Food Sci. **70:**M404–M408.
6. **Chang S-S, Lu W-YW, Park S-H, Kang D-H.** 2010. Control of foodborne pathogens on ready-to-eat roast beef slurry by ε-polylysine. Int. J. Food Microbiol. **141:**236–241. http://dx.doi.org/10.1016/j.ijfoodmicro.2010.05.021.
7. **Moschonas G, Geornaras I, Stopforth JD, Wach D, Woerner DR, Belk KE, Smith GC, Sofos JN.** 2012. Activity of caprylic acid, Carvacrol, ε-polylysine, and their combinations against *Salmonella* in not-ready-to-eat surface-browned, frozen, breaded chicken products. J. Food Sci. **77:** M405–M411. http://dx.doi.org/10.1111/j.1750-3841.2012.02757.x.
8. **Yoshida T, Nagasawa T.** 2003. ε-Poly-L-lysine: microbial production, biodegradation and application potential. Appl. Microbiol. Biotechnol. **62:**21–26. http://dx.doi.org/10.1007/s00253-003-1312-9.
9. **Yamanaka K, Maruyama C, Takagi H, Hamano Y.** 2008. ε-Poly-L-lysine dispersity is controlled by a highly unusual nonribosomal peptide synthetase. Nat. Chem. Biol. **4:**766–772. http://dx.doi.org/10.1038/nchembio.125.
10. **Takehara M, Hibino A, Saimura M, Hirohara H.** 2010. High-yield production of short chain length poly(ε-L-lysine) consisting of 5–20 residues by *Streptomyces aureofaciens*, and its antimicrobial activity. Biotechnol. Lett. **32:**1299–1303. http://dx.doi.org/10.1007/s10529-010-0294-9.
11. **Hamano Y.** 2011. Occurrence, biosynthesis, biodegradation, and industrial and medical applications of a naturally occurringε-poly-L-lysine. Biosci. Biotechnol. Biochem. **75:**1226–1233. http://dx.doi.org/10.1271/bbb.110201.
12. **Shima S, Sakai H.** 1977. Polylysine produced by *Streptomyces*. Agric. Biol. Chem. **41:**1807–1809. http://dx.doi.org/10.1271/bbb1961.41.1807.
13. **Neda K, Sakurai T, Takahashi M, Aiuchi M, Ohgushi M.** 1999. Two-generation reproduction study with teratology test of ε-poly-L-lysine by dietary administration in rats. Jpn. Pharmacol. Ther. **27:**28–29.

14. **Kido Y, Hiramoto S, Murao M, Horio Y, Miyazaki T, Kodama T, Nakabou Y.** 2003. Epsilon-polylysine inhibits pancreatic lipase activity and suppresses postprandial hypertriacylglyceridemia in rats. J. Nutr. **133:** 1887–1891.
15. **Russell AD.** 2002. Mechanisms of antimicrobial action of antiseptics and disinfectants: an increasingly important area of investigation. J. Antimicrob. Chemother. **49:**597–599. http://dx.doi.org/10.1093/jac/49.4.597.
16. **Vaara M.** 1992. Agents that increase the permeability of the outer membrane. Microbiol. Rev. **56:**395–411.
17. **Nikaido H.** 1994. Prevention of drug access to bacterial targets: permeability barriers and active efflux. Science **264:**382–388. http://dx.doi.org/10.1126/science.8153625.
18. **Nikaido H.** 2003. Molecular basis of bacterial outer membrane permeability revisited. Microbiol. Mol. Biol. Rev. **67:**593–656. http://dx.doi.org/10.1128/MMBR.67.4.593-656.2003.
19. **Yeaman MR, Yount NY.** 2003. Mechanisms of antimicrobial peptide action and resistance. Pharmacol. Rev. **55:**27–55. http://dx.doi.org/10.1124/pr.55.1.2.
20. **Melo MN, Ferre R, Castanho MARB.** 2009. Antimicrobial peptides: linking partition, activity, and high membrane-bound concentrations. Nat. Rev. Microbiol. **7:**245–250. http://dx.doi.org/10.1038/nrmicro2095.
21. **Shai Y, Oren Z.** 2001. From "carpet" mechanism to *de novo*-designed diastereomeric cell-selective antimicrobial peptides. Peptides **22:**1629–1641. http://dx.doi.org/10.1016/S0196-9781(01)00498-3.
22. **Sengupta D, Leontiadou H, Mark AE, Marrink S-J.** 2008. Toroidal pores formed by antimicrobial peptides show significant disorder. Biochim. Biophys. Acta Biomembr. **1778:**2308–2317. http://dx.doi.org/10.1016/j.bbamem.2008.06.007.
23. **Teixeira V, Feio MJ, Bastos M.** 2012. Role of lipids in the interaction of antimicrobial peptides with membranes. Prog. Lipid Res. **51:**149–177. http://dx.doi.org/10.1016/j.plipres.2011.12.005.
24. **Glukhov E, Stark M, Burrows LL, Deber CM.** 2005. Basis for selectivity of cationic antimicrobial peptides for bacterial versus mammalian membranes. J. Biol. Chem. **280:**33960–33967. http://dx.doi.org/10.1074/jbc.M507042200.
25. **Vad BS, Bertelsen K, Johansen CH, Pedersen JM, Skrydstrup T, Nielsen NC, Otzen DE.** 2010. Pardaxin permeabilizes vesicles more efficiently by pore formation than by disruption. Biophys. J. **98:**576–585. http://dx.doi.org/10.1016/j.bpj.2009.08.063.
26. **Scallan E, Hoekstra RM, Angulo FJ, Tauxe RV, Widdowson MA, Roy SL, Jones JL, Griffin PM.** 2011. Foodborne illness acquired in the United States: major pathogens. Emerg. Infect. Dis. **17:**7–15. http://dx.doi.org/10.3201/eid1701.P11101.
27. **Jadhav S, Shah R, Bhave M, Palombo EA.** 2013. Inhibitory activity of yarrow essential oil on *Listeria* planktonic cells and biofilms. Food Control **29:**125–130. http://dx.doi.org/10.1016/j.foodcont.2012.05.071.
28. **Baba T, Ara T, Hasegawa M, Takai Y, Okumura Y, Baba M, Datsenko KA, Tomita M, Wanner BL, Mori H.** 2006. Construction of *Escherichia coli* K-12 in-frame, single-gene knockout mutants: the Keio collection. Mol. Syst. Biol. **2:**2006.2008. http://dx.doi.org/10.1038/msb4100050.
29. **Miles AA, Misra SS, Irwin JO.** 1938. The estimation of the bactericidal power of the blood. Epidemiol. Infect. **38:**732–749.
30. **Meyer RL, Zhou X, Tang L, Arpanaei A, Kingshott P, Besenbacher F.** 2010. Immobilisation of living bacteria for AFM imaging under physiological conditions. Ultramicroscopy **110:**1349–1357. http://dx.doi.org/10.1016/j.ultramic.2010.06.010.
31. **Watson ML.** 1958. Staining of tissue sections for electron microscopy with heavy metals. J. Biophys. Biochem. Cytol. **4:**475–478. http://dx.doi.org/10.1083/jcb.4.4.475.
32. **Reynolds ES.** 1963. The use of lead citrate at high pH as an electron-opaque stain in electron microscopy. J. Cell Biol. **17:**208–212. http://dx.doi.org/10.1083/jcb.17.1.208.
33. **Angelova MI, Dimitrov DS.** 1986. Liposome electroformation. Faraday Discussions Chem. Soc. **81:**303–311. http://dx.doi.org/10.1039/dc9868100303.
34. **Najjar MB, Kashtanov D, Chikindas ML.** 2007. ε-Poly-L-lysine and nisin A act synergistically against Gram-positive food-borne pathogens *Bacillus cereus* and *Listeria monocytogenes*. Lett. Appl. Microbiol. **45:**13–18. http://dx.doi.org/10.1111/j.1472-765X.2007.02157.x.
35. **Ye R, Xu H, Wan C, Peng S, Wang L, Xu H, Aguilar ZP, Xiong Y, Zeng Z, Wei H.** 2013. Antibacterial activity and mechanism of action of ε-poly-L-lysine. Biochem. Biophys. Res. Commun. **439:**148–153. http://dx.doi.org/10.1016/j.bbrc.2013.08.001.
36. **Chang V, Chen L-Y, Wang A, Yuan X.** 2010. The effect of lipopolysaccharide core structure defects on transformation efficiency in isogenic *Escherichia coli* BW25113 *rfaG*, *rfaP*, and *rfaC* mutants. J. Exp. Microbiol. Immunol. **14:**101–107.
37. **Vaara M, Vaara T.** 1983. Polycations as outer membrane-disorganizing agents. Antimicrob. Agents Chemother. **24:**114–122. http://dx.doi.org/10.1128/AAC.24.1.114.
38. **Yethon JA, Heinrichs DE, Monteiro MA, Perry MB, Whitfield C.** 1998. Involvement of *waaY*, *waaQ*, and *waaP* in the modification of *Escherichia coli* lipopolysaccharide and their role in the formation of a stable outer membrane. J. Biol. Chem. **273:**26310–26316. http://dx.doi.org/10.1074/jbc.273.41.26310.
39. **Yethon JA, Vinogradov E, Perry MB, Whitfield C.** 2000. Mutation of the lipopolysaccharide core glycosyltransferase encoded by *waaG* destabilizes the outer membrane of *Escherichia coli* by interfering with core phosphorylation. J. Bacteriol. **182:**5620–5623. http://dx.doi.org/10.1128/JB.182.19.5620-5623.2000.
40. **Allende D, McIntosh TJ.** 2003. Lipopolysaccharides in bacterial membranes act like cholesterol in eukaryotic plasma membranes in providing protection against melittin-induced bilayer lysis. Biochemistry **42:**1101–1108. http://dx.doi.org/10.1021/bi026932s.
41. **Danese PN, Pratt LA, Kolter R.** 2000. Exopolysaccharide production is required for development of *Escherichia coli* K-12 biofilm architecture. J. Bacteriol. **182:**3593–3596. http://dx.doi.org/10.1128/JB.182.12.3593-3596.2000.
42. **Lee SM, Chen J.** 2004. Survival of *Escherichia coli* O157:H7 in set yogurt as influenced by the production of an exopolysaccharide, colanic acid. J. Food Prot. **67:**252–255.
43. **Postupalenko VY, Shvadchak VV, Duportail G, Pivovarenko VG, Klymchenko AS, Mély Y.** 2011. Monitoring membrane binding and insertion of peptides by two-color fluorescent label. Biochim. Biophys. Acta Biomembr. **1808:**424–432. http://dx.doi.org/10.1016/j.bbamem.2010.09.013.
44. **Schmidt NW, Mishra A, Lai GH, Davis M, Sanders LK, Tran D, Garcia A, Tai KP, McCray PB, Ouellette AJ, Selsted ME, Wong GCL.** 2011. Criterion for amino acid composition of defensins and antimicrobial peptides based on geometry of membrane destabilization. J. Am. Chem. Soc. **133:**6720–6727. http://dx.doi.org/10.1021/ja200079a.
45. **Bo T, Liu M, Zhong C, Zhang Q, Su QZ, Tan ZL, Han PP, Jia SR.** 2014. Metabolomic analysis of antimicrobial mechanisms of ε-poly-L-lysine on *Saccharomyces cerevisiae*. J. Agric. Food Chem. **62:**4454–4465. http://dx.doi.org/10.1021/jf500505n.
46. **Epand RM, Epand RF.** 2009. Domains in bacterial membranes and the action of antimicrobial agents. Mol. Biosyst. **5:**580–587. http://dx.doi.org/10.1039/b900278m.
47. **Fischer W, Leopold K.** 1999. Polar lipids of four *Listeria* species containing L-lysylcardiolipin, a novel lipid structure, and other unique phospholipids. Int. J. Syst. Bacteriol. **49:**653–662. http://dx.doi.org/10.1099/00207713-49-2-653.
48. **Tack BF, Sawai MV, Kearney WR, Robertson AD, Sherman MA, Wang W, Hong T, Boo LM, Wu H, Waring AJ, Lehrer RI.** 2002. SMAP-29 has two LPS-binding sites and a central hinge. Eur. J. Biochem. **269:**1181–1189. http://dx.doi.org/10.1046/j.0014-2956.2002.02751.x.
49. **Schmidtchen A, Malmsten M.** 2013. Peptide interactions with bacterial lipopolysaccharides. Curr. Opin. Colloid Interface Sci. **18:**381–392. http://dx.doi.org/10.1016/j.cocis.2013.06.003.
50. **Walker SL, Redman JA, Elimelech M.** 2004. Role of cell surface lipopolysaccharides in *Escherichia coli* K-12 adhesion and transport. Langmuir **20:**7736–7746. http://dx.doi.org/10.1021/la049511f.
51. **Burks GA, Velegol SB, Paramonova E, Lindenmuth BE, Feick JD, Logan BE.** 2003. Macroscopic and nanoscale measurements of the adhesion of bacteria with varying outer layer surface composition. Langmuir **19:**2366–2371. http://dx.doi.org/10.1021/la026375a.
52. **Boman HG, Monner DA.** 1975. Characterization of lipopolysaccharides from *Escherichia coli* K-12 mutants. J. Bacteriol. **121:**455.
53. **Yanisch-Perron C, Vieira J, Messing J.** 1985. Improved M13 phage cloning vectors and host strains: nucleotide sequences of the M13mpl8 and pUC19 vectors. Gene **33:**103–119. http://dx.doi.org/10.1016/0378-1119(85)90120-9.
54. **Datsenko KA, Wanner BL.** 2000. One-step inactivation of chromosomal genes in *Escherichia coli* K-12 using PCR products. Proc. Natl. Acad. Sci. U. S. A. **97:**6640–6645. http://dx.doi.org/10.1073/pnas.120163297.

55. **Chao Y, Zhang T.** 2011. Probing roles of lipopolysaccharide, type 1 fimbria, and colanic acid in the attachment of *Escherichia coli* strains on inert surfaces. Langmuir **27:**11545–11553. http://dx.doi.org/10.1021/la202534p.
56. **Parker CT, Pradel E, Schnaitman CA.** 1992. Identification and sequences of the lipopolysaccharide core biosynthetic genes *rfaQ*, *rfaP*, and *rfaG* of *Escherichia coli* K-12. J. Bacteriol. **174:**930–934.
57. **Gronow S, Brabetz W, Brade H.** 2000. Comparative functional characterization *in vitro* of heptosyltransferase I (WaaC) and II (WaaF) from *Escherichia coli*. Eur. J. Biochem. **267:**6602–6611. http://dx.doi.org/10.1046/j.1432-1327.2000.01754.x.
58. **Ruiz N, Gronenberg LS, Kahne D, Silhavy TJ.** 2008. Identification of two inner-membrane proteins required for the transport of lipopolysaccharide to the outer membrane of *Escherichia coli*. Proc. Natl. Acad. Sci. U. S. A. **105:**5537–5542. http://dx.doi.org/10.1073/pnas.0801196105.
59. **Meredith TC, Mamat U, Kaczynski Z, Lindner B, Holst O, Woodard RW.** 2007. Modification of lipopolysaccharide with colanic acid (M-antigen) repeats in *Escherichia coli*. J. Biol. Chem. **282:**7790–7798. http://dx.doi.org/10.1074/jbc.M611034200.
60. **Gottesman S, Trisler P, Torres-Cabassa A.** 1985. Regulation of capsular polysaccharide synthesis in *Escherichia coli* K-12: characterization of three regulatory genes. J. Bacteriol. **162:**1111–1119.